Metallophysics and Advanced Technologies
Металофіз. новітні технол.
Metallofiz. Noveishie Tekhnol.
2024, vol. 46, No.10, pp. 1007–1030
https://doi.org/10.15407/mfint.46.10.1007
Reprints available directly from the publisher

PACS numbers: 61.50.Ks, 61.72.Ff, 68.55.jm, 68.60.Bs, 68.65.Ac, 81.15.Jj, 81.70.Pg

Correlation of the Modulation Period and the Phase Formation in Multilayer Eutectic Al/Cu Foils

S. Polishchuk[*], A. Ustinov[**], Ya. Matvienko[*], S. Demchenkov[**], M. Skoryk[*], I. Zahorulko[*], O. Molebny[*], A. Kotko[***]

[*]*G. V. Kurdyumov Institute for Metal Physics, N.A.S. of Ukraine, 36 Academician Vernadsky Blvd., UA-03142 Kyiv, Ukraine*
[**]*E. O. Paton Electric Welding Institute, 11 Kazymyr Malevych Str. UA-03150 Kyiv, Ukraine*
[***]*I. M. Frantsevich Institute for Problems in Materials Science, N.A.S. of Ukraine, 3 Omeljan Pritsak Str., UA-03142 Kyiv, Ukraine*

Multilayer Al/Cu foils have a high potential to be used as filler materials for diffusion welding or friction stir welding of difficult-to-weld materials. In this work, we study EB-PVD-deposited multilayer Al/Cu foils with the modulation periods (sum thickness of one Al layer and one Cu layer) of 50 nm and 1000 nm. The total composition for both the foils is of about Al–30 wt.% Cu and the total thickness is varied from 20 μm to 30 μm. The phase formations within the foils during heating up to 500°C are investigated by x-ray diffractometry, scanning and transmission electron microscopies, differential scanning calorimetry, and electrical-resistance measurement. The correlation between the modulation period and the formation of the Al_2Cu, $AlCu_3$, and Al_4Cu_9 phases is studied. The sequence, temperatures, and kinetics of phase transformations, as well as the heat of the reactions, are found to correlate significantly with the modulation period. Mechanisms of the phase formations within the foils and their mechanical properties are discussed.

Key words: nanoscale Al/Cu multilayers, intermetallic compounds, texture, calorimetry, hardness.

Corresponding author: Sergiy Polishchuk
E-mail: serg.polis7@gmail.com

Citation: S. Polishchuk, A. Ustinov, Ya. Matvienko, S. Demchenkov, M. Skoryk, I. Zahorulko, O. Molebny, and A. Kotko, Correlation of the Modulation Period and the Phase Formation in Multilayer Eutectic Al/Cu Foils, *Metallofiz. Noveishie Tekhnol.*, **46**, No. 10: 1007–1030 (2024). DOI: 10.15407/mfint.46.10.1007

Багатошарові Al/C-фолії є перспективними для використання як присадкові матеріяли для дифузійного зварювання або зварювання тертям матеріялів, що важко зварюються. У цій роботі досліджено багатошарові фолії з періодами модуляції (сумарна товщина одного шару Al і одного шару Cu) у 50 нм і 1000 нм, одержані методою електронно-променевого осадження. Загальний склад для обох фолій становив приблизно Al–30 мас.% Cu, а загальна товщина — 20–30 мкм. Фазоутворення у фоліях під час нагрівання до 500°C досліджено методами рентґенівської дифрактометрії, сканувальної та трансмісійної електронних мікроскопій, диференційної сканувальної калориметрії та шляхом міряння електричного опору. Досліджено кореляцію між періодом модуляції й утворенням фаз Al_2Cu, $AlCu_3$ й Al_4Cu_9. Встановлено, що послідовність, температури та кінетика фазових перетворень, а також тепловий ефект реакцій істотно корелюють із періодом модуляції. Розглянуто можливі механізми фазоутворення у фоліях та їхні механічні властивості.

Ключові слова: багатошарові Al/Cu-фолії, інтерметаліди, текстура, калориметрія, твердість.

(Received 6 August, 2024; in final version, 1 September, 2024)

1. INTRODUCTION

Multilayer Al/Cu foils with a composition of Al–33 wt.% Cu are believed to be promising for use as filler materials for welding difficult-to-weld materials [1]. The advantage of using this Al/Cu multilayer system, as compared to Al/Ni and Al/Ti foils, lies in the lower temperature at which phase transformations begin [2]. In particular, phase transformations in such foils with submicron layer thickness were found in the temperature range of 130–360°C [3]. In addition, metastable structures often form during the annealing of multilayer films fabricated by physical vapour deposition, due to the significant density of interphase boundaries [4] and the special reaction kinetics in them [5]. Particularly, the primary formation of the tetragonal θ-Al_2Cu phase, and then the cubic γ_2-Al_4Cu_9 [6–9] or monoclinic η-AlCu phase [10, 11] was observed during the annealing of multilayer condensates of the Al/Cu system. Moreover, Vandenberg and Hamm [12] reported that, in addition to the first formed Al_2Cu phase in bilayer films, an ordered f.c.c. phase β_1-$AlCu_3$ with a lattice parameter close to 0.5801 nm formed. This high-temperature phase occurs after the Al_2Cu phase and is a secondary phase throughout the investigated range of Cu concentrations (from 33 at.% to 83 at.%). At temperatures above 350°C, the phase composition of the films approaches the equilibrium: $Al_2Cu + AlCu$. In another study, the authors [13] observed the formation of the β_1-$AlCu_3$ and γ_2-Al_4Cu_9 phases during slow (0.4°C/min) and rapid heating to the relevant annealing temperatures, respectively. It is important to mention that the disordered β-$AlCu_3$ phase ($a_0 = 0.290$

nm) serves as the parent structure from which both the β_1-$AlCu_3$ phase ($a = 0.5801$ nm $\cong 2a_0$) and the γ_2-Al_4Cu_9 phase ($a = 0.8703$ nm $\cong 3a_0$) originate [13]. It is also known that, in massive Cu–Al alloys, depending on the cooling rate, either the β_1- or γ_2-phase is formed [14].

On the other hand, the γ_2-Al_4Cu_9 phase is considered in works [15–17] as a superstructure of the β-AlCu phase of the structural CsCl type and an approximant of icosahedral quasi-crystals of the Al–Cu–Fe system [17]. This phase is characterized by a concentration of electrons close to quasi-crystals and contains local pseudopentagonal configurations of atoms and distorted icosahedrons [15]. The cubic phase γ_2-Al_4Cu_9 is stable at low temperatures, and its stabilization is associated with the Hume-Rothery mechanism, similar to that is observed for the icosahedral phase. At the same time, the number of atoms per unit cell (52 atoms) is significantly greater than in ordinary metals but less than in most approximants. In addition, besides a cubic γ_2-Al_4Cu_9 phase with a lattice parameter $a_{\gamma 2} = 0.860$ nm, metastable cubic β and β_1 phases with lattice parameters $a = 0.287$ nm and 0.572 nm, respectively, were also found [15]. Furthermore, the ratio between the parameters of these cubic phases was noted: $a_{\gamma 2} \cong 3a_\beta$ and $a_{\beta 1} \cong 2a_\beta$ [15]. Even though the γ_2-Al_4Cu_9 phase has a complex structure, it is formed in a wide concentration range. To explain the mechanism of formation of the b.c.c. γ_2-Al_4Cu_9 phase, Besson *et al.* [18] proposed a model of its formation from a solid solution of f.c.c. Al(Cu) by a shear mechanism, which can be considered as a classical (uniaxial) Bain transformation.

While phase transformations in the Al/Cu multilayer system were extensively investigated, variations in their sequence and kinetics can be related to factors such as modulation period, heating rates, grain sizes, and the relative orientations between phases. In addition, from the point of view of using these foils as the filler materials for diffusion welding, it is of practical interest to study the influence of their modulation period on the plasticity coefficient after annealing at different temperatures. Therefore, this work aimed to study the effect of the modulation period on the sequence of phase transformations, the thermal characteristics of the reactions, and the mechanical properties of Al/Cu eutectic foils obtained by physical vapour deposition.

2. EXPERIMENTAL

Al/Cu multilayer foils of two types, *A* and *B* with a modulation period λ of 50 nm and 1000 nm, respectively, were produced by the layer-by-layer electron beam deposition of components on a substrate rotating at a constant speed. During this process, evaporation from aluminium and copper sources separated by an impermeable screen occurs [3]. The varying intensities of aluminium and copper vapour flow, as well as the substrate rotation rate, allow the deposition of Al/Cu multilayer foils with

different thicknesses of elemental layers. To obtain self-standing condensates, a layer of CaF_2 salt was first deposited on the steel substrate, thus enabling easy separation of the foil from the substrate later on. Chamber pressure was $5 \cdot 10^{-3}$ Pa. Evaporation intensity provided the deposition rate of 50 nm/s and substrate temperature during deposition was in the range of 90–100°C. The total composition for both types of foils was close to the eutectic Al–30 wt.% Cu and the total thickness was in the 20–30 μm range. The foils were annealed in a furnace at the residual pressure of 10^{-1} Pa. The temperature intervals of phase transformations in multilayer foils were determined using the differential scanning calorimetry (DSC). The thermal signal from the samples was recorded using a NetzschDSC 404 F1 Pegasus calorimeter in the temperature ranges of 20–550°C in the heating mode at a rate of 40, 20, 10, 5 K/min in an atmosphere of 99.99% helium. X-ray diffraction studies of multilayer foils were carried out using a DRON-4 diffractometer using CuK_α radiation. Lattice parameters of Al were determined according to positions of (220), (311) and (222) peaks. The texture analysis of foils was conducted using an x-ray DRON-3 diffractometer with a texture attachment in CoK_α radiation. The measurement was carried out using parallel beam geometry and scan angles from 0° to 80° and from 0° to 360° for α and β, respectively. Data collected on a textureless $BaTiO_3$ specimen were used to take into account the defocusing effect. The analysis of the crystallographic texture was carried out by constructing pole figures (PFs) using the MTEX MATLAB software package [19]. Microstructures of cross-sections of as-deposited and annealed multilayered Al/Cu foils were analysed with a TESCAN MIRA facility equipped with an In-Beam SE detector. Planar-TEM of the annealed foils was performed using a JEM-2000FXII. Measurements of electrical resistivity were performed in automatic mode on foils 50 mm long and 1–2 mm wide during their continuous heating with the heating rates of 3°C/min in the range from 20°C to 500°C. The reduced temperature coefficient of electrical resistance $\alpha = R_0^{-1} dR/dT$ was also determined, where R_0 is the initial resistance of the foil at room temperature.

Mechanical properties of multilayer foils were studied using a universal differential nanoindenter "Micron-Gamma" at the 30 g loading. The Meier microhardness (HM), Young's modulus (E), and the plasticity coefficient for the material were determined using the indentation data [20].

3. RESULTS AND DISCUSSION

3.1. Changes in the Structure of Al/Cu Multilayer Foils During Annealing

The cross-sectional microstructures of deposited foils with modulation periods of 50 and 1000 nm are shown in Fig. 1. It can be seen that the

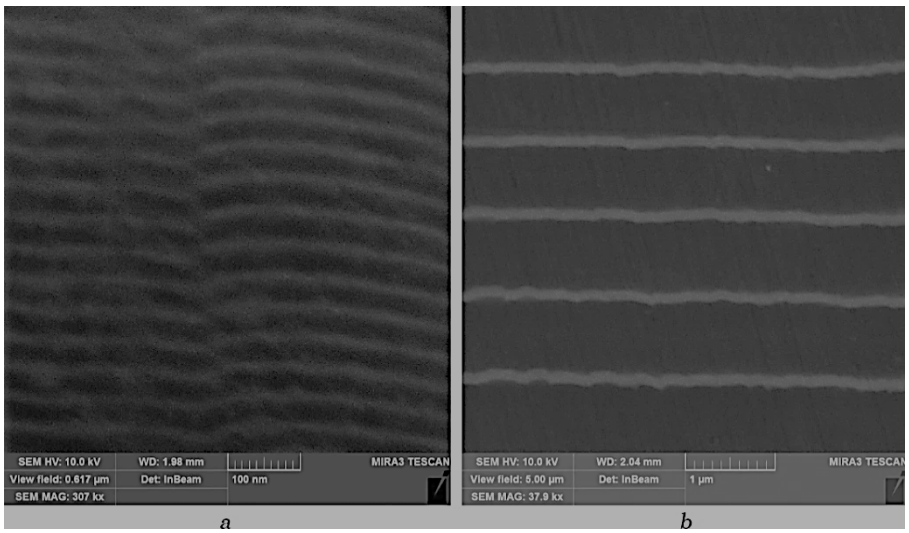

Fig. 1. Microstructure of the cross-section of Al–30 wt.% Cu multilayer foils of two types: *A*—with a modulation period, $h \cong 50$ nm (*a*) and *B*—with $h \cong 1000$ nm (*b*).

foils after deposition consist of continuous layers of copper (light) and aluminium (dark) with some areas with grey contrast, which can be considered as the result of mixing of atoms between the layers. From the analysis of diffraction patterns of the foils in an as-deposited state and after annealing's at different temperatures for 30 minutes (Fig. 2), it is clear that, in the case of a short modulation period (50 nm), the formation of the Al_2Cu phase occurs in the foils even during the deposition process, *i.e.*, at temperatures in the 90–100°C range. At the same time, parallel growth of the Al_2Cu phase and the metastable Al_4Cu_9 phase is already observed at 130°C.

The appearance of the Al_4Cu_9 phase in the foil is accompanied by a sharp decrease in the copper phase fraction and further rapid growth of this phase is observed until a temperature of 150°C is reached, after which its volume fraction decreases and eventually disappears in the temperature range from 200°C to 250°C.

In foils with $\lambda = 1000$ nm, in the initial state, there are no peaks from the Al_2Cu phase, and the appearance of the weak peaks of both Al_2Cu and A_4Cu_9 are observed at $T = 135$°C, after which their volume fractions gradually increase. Moreover, peaks of the β_1-$AlCu_3$ cubic phase with a lattice parameter $a = 0.5801$ nm are observed at $T = 215$°C. It should be noted that this phase was previously observed in Ref. [12] and its diffraction pattern (Fig. 3) contains intense peaks (111) and (311) at angles $2\theta = 26.8°$ and 52.5°, respectively, which distinguishes it from the Al_4Cu_9 phase.

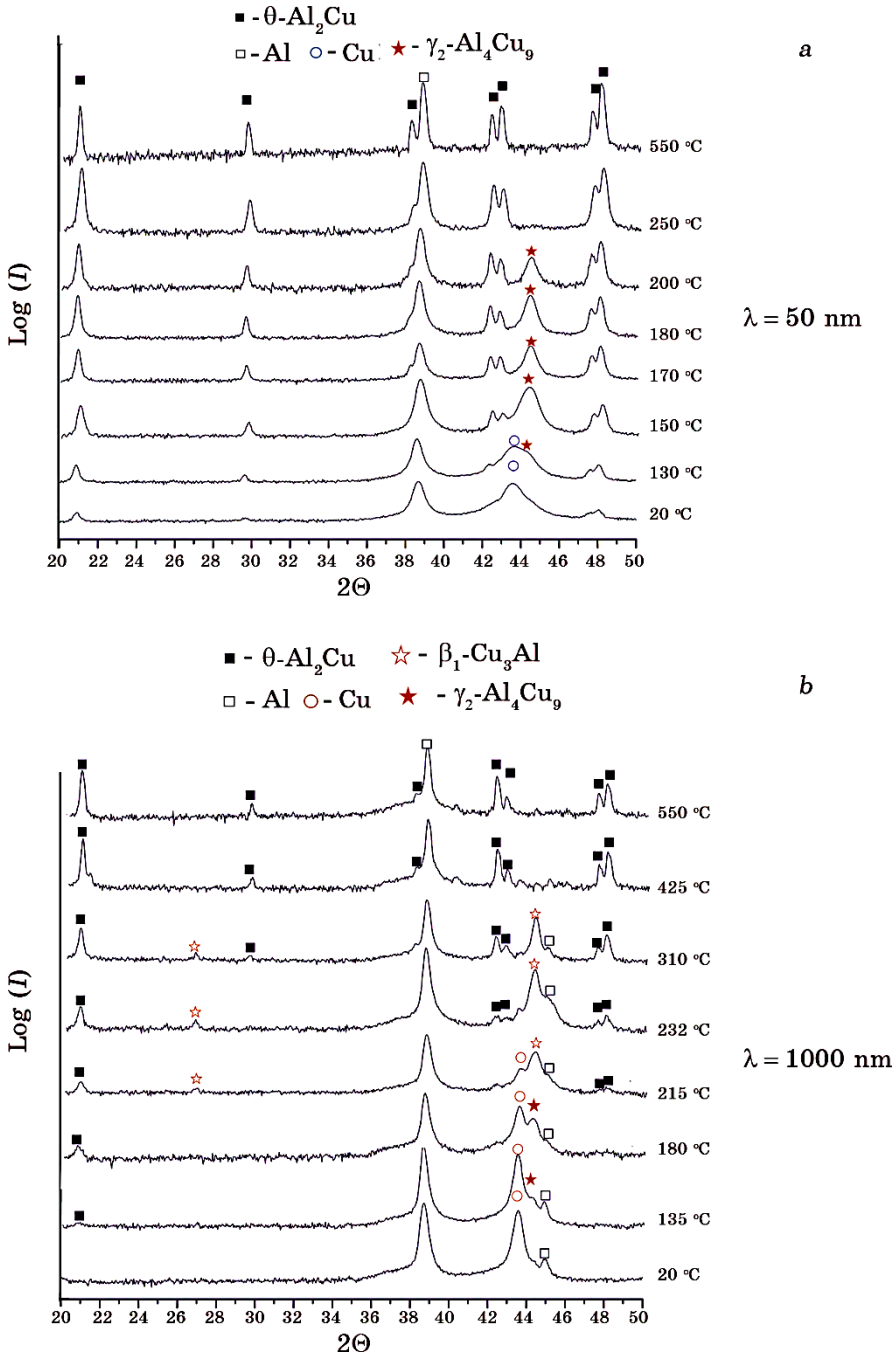

Fig. 2. Diffraction patterns from foils with a modulation period of 50 nm (*a*) and 1000 nm (*b*) after annealing at different temperatures.

Yet, we can suppose that the foil contains a mixture of these $AlCu_3$ and Al_4Cu_9 phases. The mix of the $AlCu_3$ and Al_4Cu_9 phases grows to a temperature of 245°C, after which its volume fraction decreases, and at 425°C, it completely disappears. Annealing at higher temperatures approach the phase composition of the film to the equilibrium one: $Al + Al_2Cu$.

From the analysis of changes in the diffraction patterns of studied foils during the annealing process (Fig. 2), we can conclude that in both cases the θ-Al_2Cu phase forms first and grows gradually with temperature (Fig. 4).

The further γ_2-Al_4Cu_9 phase appears at temperatures of about 130°C also for both these foils. For the foil with the ling modulation period (1000 nm), in addition to the Al_2Cu and A_4Cu_9, the β_1-$AlCu_3$ phase forms at the temperature range of 180–215°C. Further rapid growth of the A_4Cu_9 and β_1-$AlCu_3$ phases occurs up to temperatures of 150°C and 235°C, respectively, where their volume fractions are maximal.

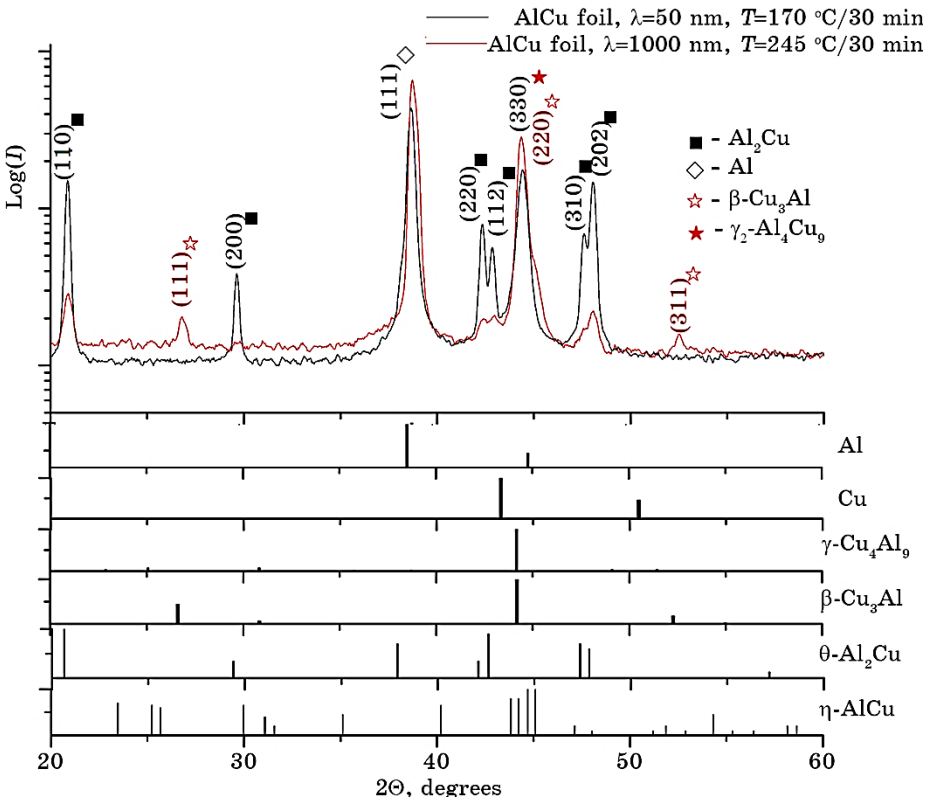

Fig. 3. X-ray diffraction patterns of foils with a modulation period of 50 nm and 1000 nm after annealing at temperatures of 170°C and 245°C, respectively.

It should be noted that the growth of the γ_2-Al_4Cu_9 and β_1-$AlCu_3$ phases is accompanied by a slight increase in the volume fraction of the

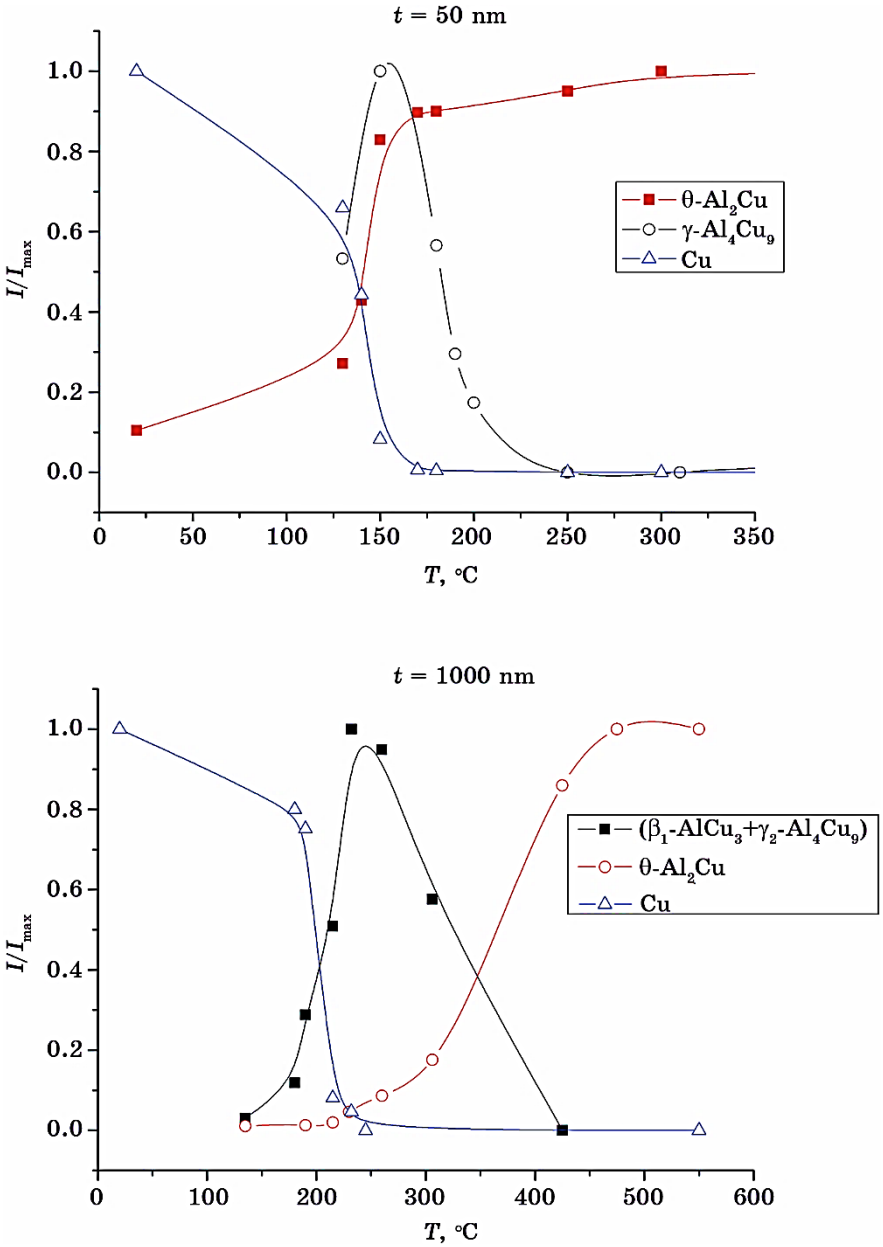

Fig. 4. Change in the relative intensities of diffraction peaks of Cu and the Al_2Cu, Al_4Cu_9, and β_1-$AlCu_3$ phases depending on temperature.

θ-Al_2Cu phase. This suggests that these phases grow in parallel. On the contrary, the growth of the γ_2-Al_4Cu_9 and β_1-$AlCu_3$ phases is accompanied by a sharp decrease in the copper content in the foils. Thus, we can suppose a two-channel transformation scheme in Al/Cu foils: (1) The θ-Al_2Cu phase forms from a supersaturated solid solution of Al(Cu) due to the diffusion of copper atoms into aluminium; (2) The remaining copper forms a Cu(Al) solid solution, which, through reaction interaction with aluminium, leads to the formation of the γ_2-Al_4Cu_9. In the case of the long-period foil, the β_1-$AlCu_3$ phase forms additionally.

It is known that the formation of intermetallic compounds in Al–Cu foils leads to a change in their electrical resistivity [9]. Figure 5 shows the dependence of the electrical resistance of studied foils on temperature at a heating rate of 3°C/min. It can be seen that the change in electrical resistance of foil with a short modulation period occurs at lower temperatures compared to foils with a long period. Local maximums of electrical resistance are observed at temperatures of 150° and 230–260°C for the foils with λ of 50 nm and 1000 nm, which corresponds to the maximum content of the metastable γ_2-Al_4Cu_9 or β_1-$AlCu_3$ phase. These metastable phases have an electrical resistance approximately 2 times greater than that of the Al_2Cu phase [21] and their decomposition leads to a decrease in the temperature coefficient of electrical resistance at temperatures in the 160–190°C range for the foil with λ of 50 nm and in the 230–300°C range for the foil with λ of 1000 nm. In the latter case, there is an additional increase in the temperature coefficient of electrical resistance followed by a subsequent decrease within the temperature range of 300°C to 400°C. This behaviour can likely be attributed to the interplay of two factors: the decomposition of the β_1-$AlCu_3$ phase and an increase in the volume fraction of the θ-Al_2Cu phase. Above 410°C, the β_1-$AlCu_3$ phase vanishes, and the subsequent

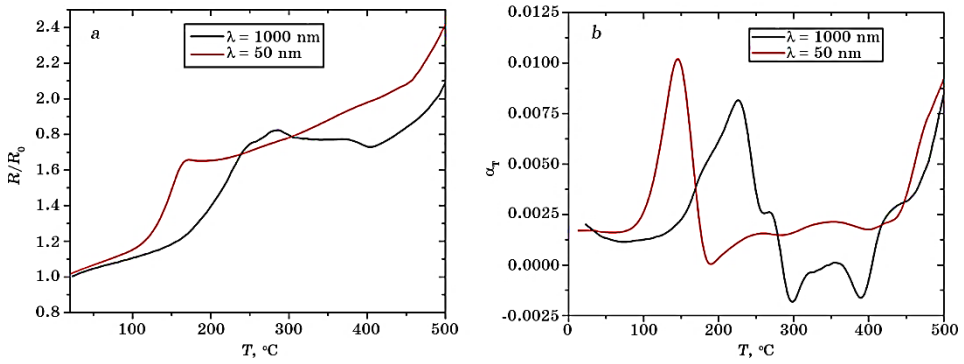

Fig. 5. Temperature dependence of electrical resistance (*a*) and temperature coefficient of electrical resistance (*b*) for foils with modulation periods of 50 and 1000 nm.

behaviour of the temperature coefficient of electrical resistance is influenced by the phase composition, which closely resembles the equilibrium Al + Al_2Cu composition.

From the images of the microstructure of the foil obtained using transmission electron microscopy (Fig. 6), it is clear that both aluminium and the Al_2Cu phase in the foil with $\lambda = 50$ nm after annealing at a temperature of 150°C have nanostructured grains of 50–100 nm. The distribution of reflections in the electron diffraction pattern of this foil proves the presence of Al, Al_2Cu, and Al_4Cu_9 phases. It should be noted that the presence of a superstructure reflection (210) in the electron diffraction pattern indicates the partial ordering of the Al_4Cu_9 phase in the foil [18].

As can be seen from Fig. 7, the foil with $\lambda = 1000$ nm after annealing at a temperature of 200°C contains aluminium crystallites of 150–300 nm in size and Al_2Cu intermetallic of 70–200 nm in size.

The distribution of reflections in the electron diffraction pattern of this foil indicates the presence of Al, Al_2Cu, and $AlCu_3$ phases. The absence of reflections of the Al_4Cu_9 phase for this foil suggests this phase

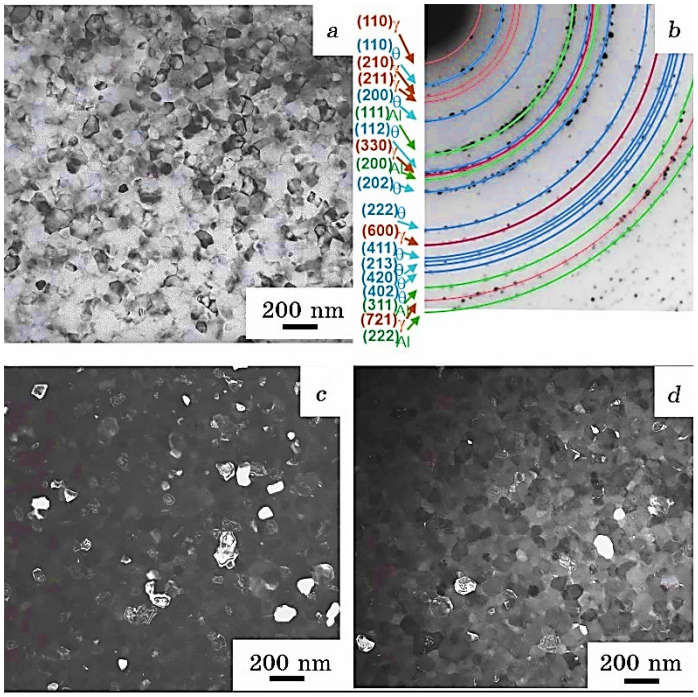

Fig. 6. Bright field (*a*), electron diffraction pattern (*b*), dark field in reflections of aluminium (*c*) and Al_2Cu phase (*d*) from the Al–30 wt.% Cu foil with a layer period of 50 nm after annealing at 150°C.

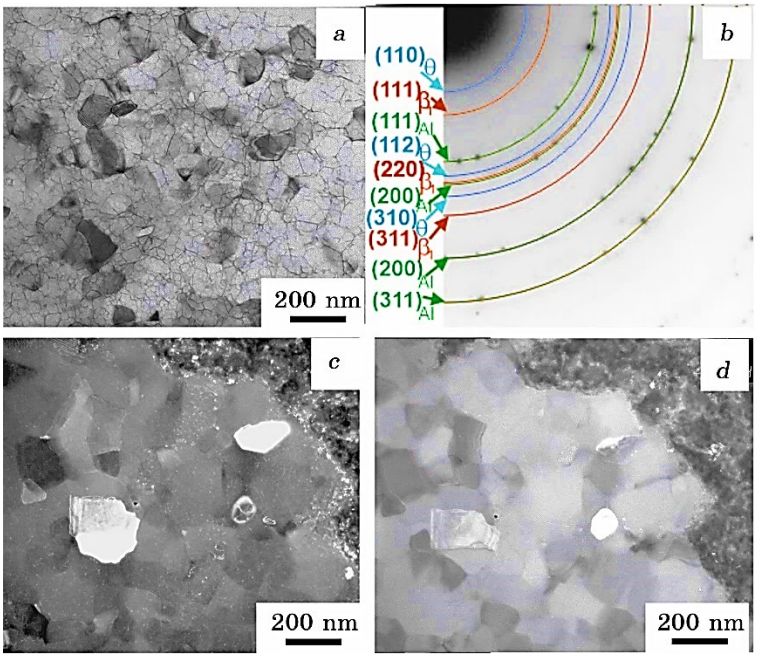

Fig. 7. Bright field (*a*), electron diffraction pattern (*b*), dark field in reflections of aluminium (*c*) and Al_2Cu phase (*d*) from the Al–30 wt.% Cu foil with a modulation period of 1000 nm after annealing at a temperature of 200°C.

disappeared after annealing at 200°C.

The lattice parameter a_{Al} was calculated from the positions of the (220), (311) and (222) peaks of aluminium in the diffraction patterns of studied foils in the initial state and after annealing. It was found that, for the foil with $\lambda = 1000$ nm after annealing at 150°C, it decreases from 0.4049 nm to 0.4044 nm (Fig. 8), which is probably due to the formation of a supersaturated Al(Cu) solid solution consistent with the Al–Cu phase diagram [22]. To quantify the copper content (c_{Cu}) in it, an empirical equation from [23] was used. Thus, the value at this stage was about 2.5 at.%. Increasing the annealing temperature to 170°C leads to a sharp increase in the lattice parameter to 0.4047 nm and a decrease in the copper content in the solid solution to 0.6 at.%. A further increase in temperature up to 500°C did not significantly affect the change in the Al lattice parameter. In contrast, for the foil with $\lambda = 50$ nm in the initial state $\alpha_{Al} = 0.4043$ nm, which can be considered as the result of mixing atoms between layers and forming a supersaturated Al(Cu) solid solution with a copper content of about 3.1 at.% directly during the deposition process. Annealing of the foil at a temperature of 150°C leads to a sharp increase in the Al lattice parameter to 0.4049 nm and decomposition of the Al(Cu) solid solution. A further

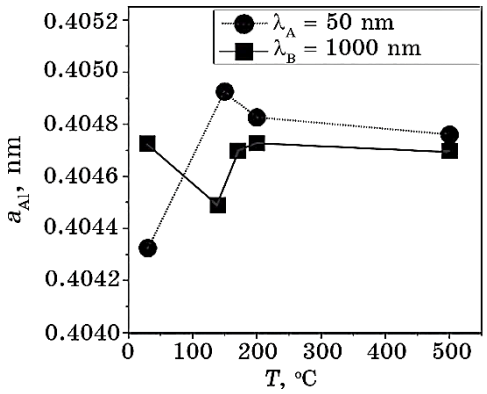

Fig. 8. Changes in the Al lattice parameter for the studied foils during the annealing process.

increase in the annealing temperature from 200°C to 500°C had an insignificant effect on the aluminium lattice parameter in these foils. Thus, the data obtained confirm the assumption of a two-channel transformation scheme in Al/Cu foils and the formation of the θ-Al_2Cu phase from Al(Cu) solid solution, as noted above. In addition, the different nature of the dependences of the aluminium lattice parameter on the annealing temperature of the studied foils also confirms the data on the different kinetics of phase formation processes in them.

3.2. Texture of Formed Phases in Al/Cu Multilayer Foils

A characteristic feature of films obtained by vacuum deposition is their texture. Figure 9 shows the PFs from Al, Cu, and the θ-Al_2Cu, γ_2-Al_4Cu_9, and β_1-$AlCu_3$ phases. PFs were constructed using reflections (111), (200), and (220) for Al and Cu, (110), (200), and (202) for θ-Al_2Cu, (330), (600) and (721) for γ_2-Al_4Cu_9 and (111), (220) and (311) for the β_1-$AlCu_3$ phase. It can be seen that in both cases, the original Al/Cu multilayer foils had a sharp axial texture <111> of both aluminium and copper layers (Fig. 4), which may be due to the lowest surface energy of the (111) planes [24]. At the same time, the resulting phases Al_2Cu, Al_4Cu_9, and β_1-$AlCu_3$ are also characterized by an axial texture. Thus, in foil with λ = 50 nm, the resulting tetragonal Al_2Cu and cubic γ_2-Al_4Cu_9 phases are characterized by an axial texture <110>. In the case of foil with λ = 1000 nm, the resulting tetragonal phase has a weak texture, while the cubic phase β_1-$AlCu_3$ has a pronounced axial texture <110>, which may indicate the formation of this phase directly from the textured copper phase.

Thus, in the case of foils with a modulation period of 50 nm, the following orientational relationships are observed between the texture

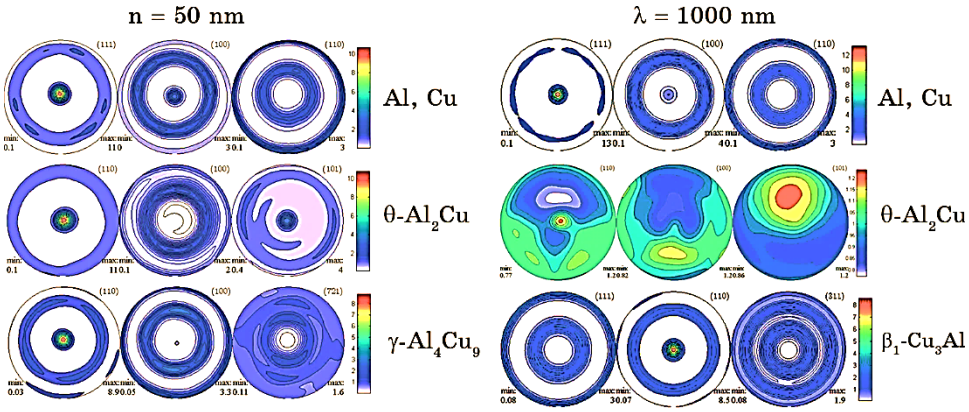

Fig. 9. PFs from Al, Cu (not shown, similar to PF from Al) and phases θ-Al_2Cu, γ_2-Al_4Cu_9 and β_1-$AlCu_3$ for foils with modulation periods of 50 nm and 1000 nm.

directions and the planes of the original aluminium, copper, and the resulting phases θ-Al_2Cu and γ_2-Al_4Cu_9:

$$\text{directions } \langle 111\rangle_{Cu} \| \langle 111\rangle_{Al} \| \langle 110\rangle_{\theta\text{-}Al_2Cu} \| \langle 110\rangle_{\gamma_2\text{-}Al_4Cu_9},$$
$$\text{planes } \{111\}_{Cu} \| \{111\}_{Al} \| \{110\}_{\theta\text{-}Al_2Cu} \| \{110\}_{\gamma_2\text{-}Al_4Cu_9}.$$

For foils with a modulation period of 1000 nm, the following relationship is observed between the initial Al, Cu and the resulting β_1-$AlCu_3$ phase:

$$\text{directions } \langle 111\rangle_{Cu} \| \langle 111\rangle_{Al} \| \langle 110\rangle_{\beta_1\text{-}AlCu_3},$$
$$\text{planes } \{111\}_{Cu} \| \{111\}_{Al} \| \{110\}_{\beta_1\text{-}AlCu_3}.$$

Several studies previously observed orientation relationships between copper and the tetragonal phase θ-Al_2Cu, as well as copper and the cubic phase γ_2-Al_4Cu_9 in Al/Cu films [25, 26]. Thus, using TEM in Ref. [24], the following orientation relationships were discovered:

$[110]_\theta \| [111]_{Cu}$ (zone axis), $(001)_\theta \| (1\bar{1}0)_{Cu}$ and $(\bar{1}10)_\theta \| (\bar{1}\bar{1}2)_{Cu}$ on the (111)Cu surface,

$[110]_\theta \| [110]_{\gamma_2}$ (zone axis), $(110)_\theta \| (112)_{\gamma_2}$ on the (111)Cu surface.

The formation of the θ-Al_2Cu phase while maintaining the orientational relationships with the initial Al and Cu can lead to a decrease in the interface energy, which significantly lowers the energy barrier to nucleation and allows the appearance of very small nuclei, thus facilitating the formation of a new phase [24]. Note also that the misfit between the θ-Al_2Cu and Al lattices on the $\{111\}Al \| \{110\}\theta$ plane in the $[110]\theta \| [110]Al$ direction is 1.23%, and in the $[001]\theta \| [112]Al$ direction, it is 1.71% [27]. Similarly, the misfit between the θ-Al_2Cu and Cu lat-

tices on the $\{111\}Cu\|\{110\}\theta$ plane in the direction $[001]_\theta\|[112]_{Cu}$ is 3.09%, and in the $[110]\theta\|[110]_{Al}$ direction, it is 4.6% [25].

In both cases, the lattice of the θ-Al_2Cu phase experiences compressive stress. Finally, it is noteworthy that of the available intermetallic compounds of the system, the θ-Al_2Cu phase has the chemical composition closest to aluminium. All these factors indicate a possible decrease in the surface energy and the energy barrier for the formation of the θ-Al_2Cu phase in Al/Cu multilayer foils while maintaining the orientational relationships between the phases.

The presence of orientational relationships between the γ_2-Al_4Cu_9, β_1-$AlCu_3$, and Cu phases also indicates a decrease in the surface energy of formation of the γ_2-Al_4Cu_9 and β_1-$AlCu_3$ phases, which may facilitate their formation in comparison with the η-AlCu phase. The work [25] also shows a relatively small level of misfit between the lattices of the γ_2-Al_4Cu_9 phase and copper in the $\{111\}_{Cu}\|\{110\}_{\gamma_2\text{-}Al_4Cu_9}$ planes under the condition $[110]_{Cu}\|[111]_{\gamma_2\text{-}Al_4Cu_9}$. In addition, as can be seen in Fig. 10, the Al–Al_2Cu transformation leads to a decrease in the specific volume per atom by 9.8%, and the Cu–$AlCu_3$ and Cu–Cu_9Al_4 transformations lead to its increase by 3.18% and 7.29%, respectively.

Taking into account the fact that both γ_2-Al_4Cu_9 and β_1-$AlCu_3$ phases can be considered as b.c.c.-derivative structures [13, 28, 29], it is interesting to note that the presence of orientational relationships between directions of the axial texture of the initial f.c.c. Cu(Al) phase with lattice parameter about a = 0.362 nm and the γ_2-Al_4Cu_9 phase formed by the b.c.c. phase (a = 0.8703 nm $\cong 3a_0$, a_0 = 0.290 nm) and β_1-$AlCu_3$ phase (a = 0.5801 nm $\cong 2a_0$) may also be evidence of a shear (or diffusion-shear) transformation mechanism, as it was proposed by R. Besson *et al.* in Ref. [18]. Particularly, the observed relationship $\{111\}_{Cu}\|\{110\}_{\gamma_2\beta_1}$ between directions of the textures of initial f.c.c.-

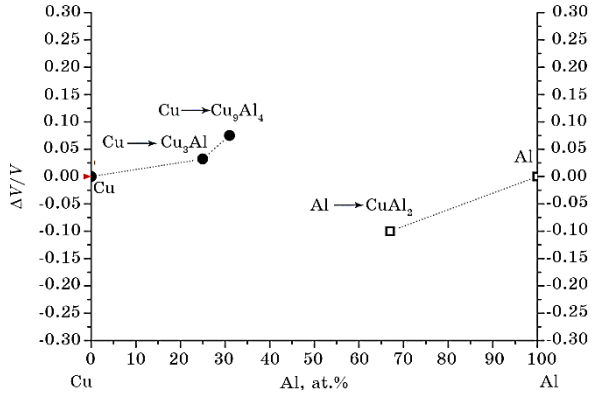

Fig. 10. Changes in the specific volume of crystalline phases during phase transformations in the Al–Cu system.

based and final b.c.c.-based structures corresponds to Kurdjumov–Sachs orientation relationship [30], and the schematic mechanism of the possible transformation is shown in Fig. 11.

It is worth noting that similar relationships between directions of textures of the initial f.c.c. phase and final b.c.c.-based phase were also observed for multilayer Cu–20 wt.% Al foils with a modulation period of 60 nm [31]. We suppose that the formation of the Al_4Cu_9 phase can occur through the following steps: (1) diffusion of Al atoms into the Cu layer and the formation of the supersaturated solid solution Cu(Al) with a local composition close to γ_2-Al_4Cu_9; (2) chemically induced instability leads to the displacive transformations from f.c.c. Cu(Al) lattice to b.c.c. lattice through the contraction by 34% along $\boldsymbol{a}_1$ axis and elongation by 14% along $\boldsymbol{a}_2$ axis; (3) chemical rearrangements and ordering of vacancies with formation of b.c.c.-derivative structures, including the γ_2-Al_4Cu_9 phase [18].

The high degree of texture for both studied foils implies their structure consists of columnar-like grains. Values of the initial Cu layer thickness are about 7 nm and 100 nm for the foils with modulation periods of 50 nm and 1000 nm, respectively. Therefore, we can assume that copper diffuses into aluminium, leading to the formation of the

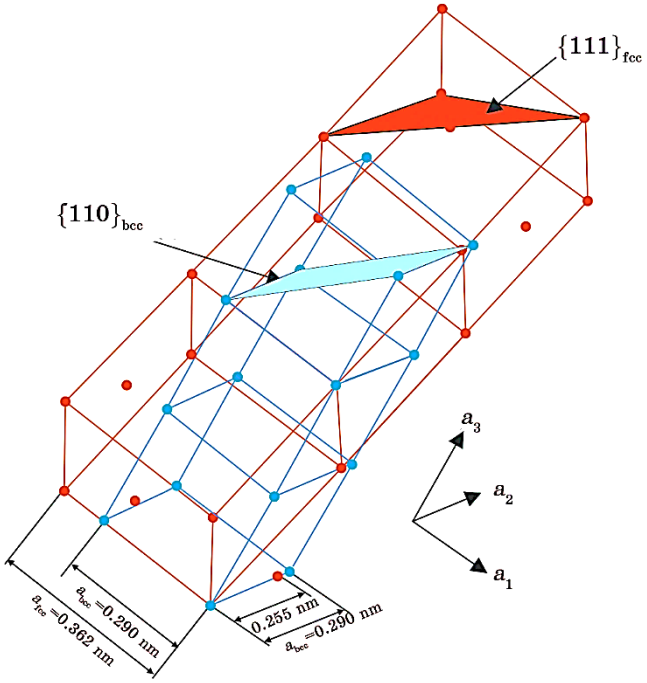

Fig. 11. Schematic illustration of the Kurdjumov–Sachs orientation relationship between the initial f.c.c. Cu(Al) and derivative from b.c.c. β-phase.

Al_2Cu phase (Fig. 12).

On the other hand, aluminium diffuses into the copper layer, forming a Cu(Al) solid solution, followed by the Al_4Cu_9 phase. The formation of both Al_2Cu and γ_2-Al_4Cu_9 predominantly takes place at the interphase boundaries between the Al and Cu layers, and between the Al_2Cu and Cu layers, respectively. The volume fraction of these phases at the interfaces is approximately 20 times greater in the short-period foils compared to the long-period foil. This fact, in particular, explains the absence or smaller fraction of γ_2-Al_4Cu_9 and Al_2Cu phases for the as-deposited long-period foil (Fig. 2, *b*).

It should be noted that the apparent copper layer thickness in the short-period foil appears to be larger due to the formation of Al_2Cu phase during the deposition. The growth of the γ_2-Al_4Cu_9 phase is restricted by consuming the Cu layer. For the case of the foil with $\lambda = 1000$ nm, the Cu layer thickness is about 100 nm and the diffusion of Al into Cu occurs via boundaries of the columnar-like grains (Fig. 12), which presumably leads to the formation of the β_1-$AlCu_3$ phase at temperatures above 180°C. The formation of the γ_2-Al_4Cu_9 or β_1-$AlCu_3$ phases can occur either by the diffusion mechanism of nucleation and growth of a new phase, in which the orientation relationships between

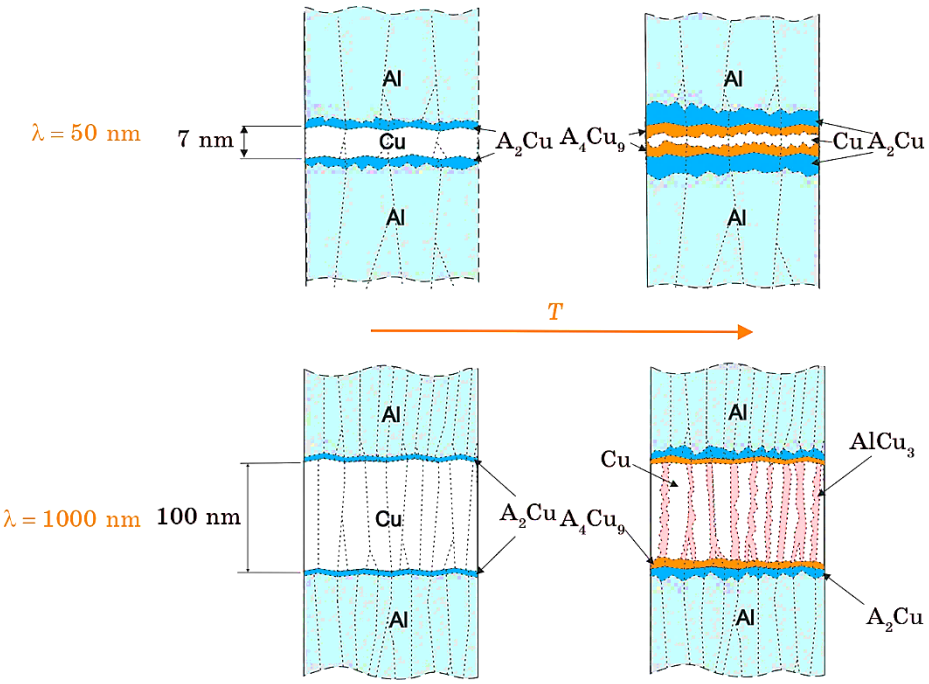

Fig. 12. Schematic diagram of initial stages of the phase formation in Cu–Al foils with modulation periods of 50 nm and 1000 nm.

the phases play an important role or by the Bain shear mechanism of transformation of the f.c.c. lattice Cu(Al) into the b.c.c. lattice γ_2-Al_4Cu_9, as proposed in Ref. [18]. In this case, as shown in [32], the driving force for such a transformation can be the chemically induced mechanical instability of the f.c.c. lattice.

It should also be emphasized that the growth of the γ_2-Al_4Cu_9 or β_1-$AlCu_3$ phases should be accompanied by an increase in the specific volume, while the parallel growth of the Al_2Cu phase occurs with a decrease in the specific volume. This circumstance, as well as the presence of excess vacancies [33] in the foils, probably reduces the level of elastic stress that arises during the growth of the γ_2-Al_4Cu_9 or β_1-$AlCu_3$ phases.

3.3. Calorimetric Study of Al/Cu Multilayer Foils

A study of the obtained foils using differential scanning calorimetry (Fig. 13, *a*) showed that the heat flux as a result of the exothermic reaction in foils with a modulation period of 50 nm is approximately 2–2.5 times higher than in foils with λ of 1000 nm. This is apparently due to the increase in the number of reaction interfaces per unit volume, which increases the rate of heat release from the reaction compared to the rate of heat dissipation. This, in turn, leads to an increase in temperature at the interface and an increase in the reaction rate. Similar results were observed when the modulation period in multilayer Ni/Si films was decreased [34]. The maxima of exothermic peaks in the DSC curves taken at a heating rate of 40°C/min corresponded to temperatures of 187.6°C and 267.4°C for foils with short and long modulation periods, respectively, which correlates with x-ray diffractometry and electrical resistivity data (Fig. 2, Fig. 5).

With an increase in the heating rate for both types of multilayer foils, a shift of the peaks towards higher temperatures is observed, which is characteristic of thermal activation processes. This shift with increasing heating rate is related to the activation energy of the reaction and can be described using the Kissinger equation [35]:

$$\ln\left(\frac{H}{T_p^2}\right) = \text{const} - \frac{E}{kT_p},$$

where H is the heating rate, T_p is the peak temperature on the DSC curve, k is Boltzmann's constant, and E is the activation energy.

For foil with a modulation period of 50 nm, when heated in the temperature range from 130°C to 150–160°C, two processes occur almost simultaneously with the formation of the θ-Al_2Cu and γ_2-Al_4Cu_9 phases, which is reflected in the nonlinear dependence of the change in the logarithm of the reaction rate on temperature (Fig. 13, *b*).

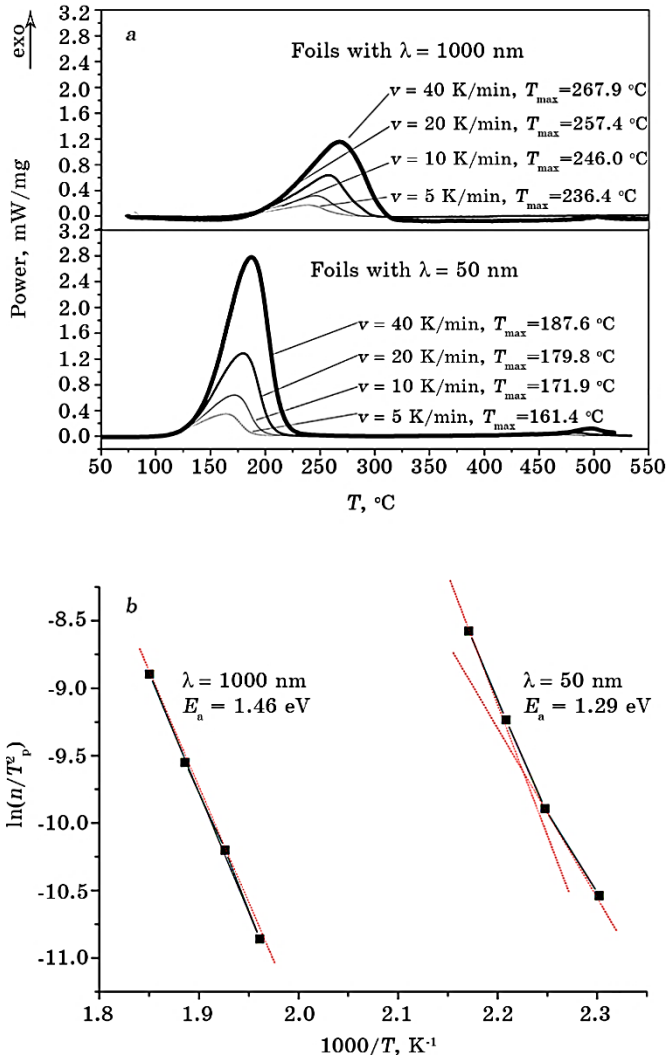

Fig. 13. DSC curves taken at different heating rates υ = 5, 10, 20, and 40 K/min for the foils with a modulation period of 50 nm and 1000 nm (*a*). Change in the logarithm of the reaction rate versus temperature for these foils.

Assuming the same reaction model for the formation processes of the θ-Al_2Cu and γ_2-Al_4Cu_9 phases, the effective activation energy, determined from the slope of the Kissinger dependence, for a process consisting of two competing reactions will be expressed as follows [36]:

$$E_{ef} = \frac{E_1 k_1(T) + E_2 k_2(T)}{k_1(T) + k_2(T)} = 124.8 \ \frac{\text{kJ}}{\text{mol}} = 1.29 \text{ eV},$$

where E_1, $k_1(T)$ and E_2, $k_2(T)$ are the activation energy and the effective reaction-rate constant for reactions with the formation of θ-Al_2Cu and γ_2-Al_4Cu_9 phases, respectively. As expected, the obtained E_{ef} value lies between reported values [13] of the activation energy for the Al_2Cu ($E_a = 1.21$ eV) and Al_4Cu_9 ($E_a = 1.59$ eV) phases.

In the case of foils with a modulation period of 1000 nm, in the temperature range from 180°C to 245°C, an increase in the β_1-$AlCu_3$ phase is observed, while the volume fraction of the θ-Al_2Cu phase remains below 10–20 vol.% (Fig. 4). The low growth rate of the θ-Al_2Cu phase may be due to the absence of orientation relationships between the formed phase and the initial Al and Cu phases (Fig. 7), which increases the interface energy and complicates the growth of this phase compared to the β_1-$AlCu_3$ phase, for which the orientation relationships are observed. In this regard, the activation energy E_{ef}, determined by the Kissinger method, for this foil can be associated with the formation reaction of the β_1-$AlCu_3$ phase. Therefore, we can estimate the activation energy of the formation reaction of the β_1-$AlCu_3$ phase as $E_{\beta_1\text{-}AlCu_3} \cong$ $\cong 141.6$ kJ/mole = 1.46 eV. The obtained value is close to the activation energy for the γ_2-Al_4Cu_9 phase reported in Ref. [13] and is higher than E_{ef} for the foil with λ = 50 nm, which confirms another mechanism of the formation for the phase. Moreover, it is worth noting that in foil with λ of 50 nm, the formation of a primary layer of Al_2Cu intermetallic compound at the interface between the aluminium and copper layers was observed during the deposition process (Fig. 2), which could affect the kinetics of further transformation.

3.4. Mechanical Characteristics of Al/Cu Multilayer Foils

It is known that the hardness of multilayer foils can significantly depend on the layer thickness, orientational epitaxy, interface structure, and deposition method. Therefore, it was of interest to study the microhardness (HM) and Young's modulus (E) of foils of different modulation periods in the initial state and after annealing (Fig. 14). It can be seen that for the foil with λ of 50 nm after deposition $HM = 4.7$ GPa ($E = 138$ GPa), which is ≅ 3 times greater than for the foil with λ of 1000 nm ($HM = 1.6$ GPa, $E = 82$ GPa). This may be explained by the action of the following strengthening mechanisms: reduced layer thickness, grain size effect, and interface alloying [37]. Annealing of the studied foils at 150°C leads to the growth of intermetallic compounds, which increases the microhardness and Young's modulus of Al/Cu multilayer foils to values of 5.6 GPa and 147 GPa for the foil with λ of

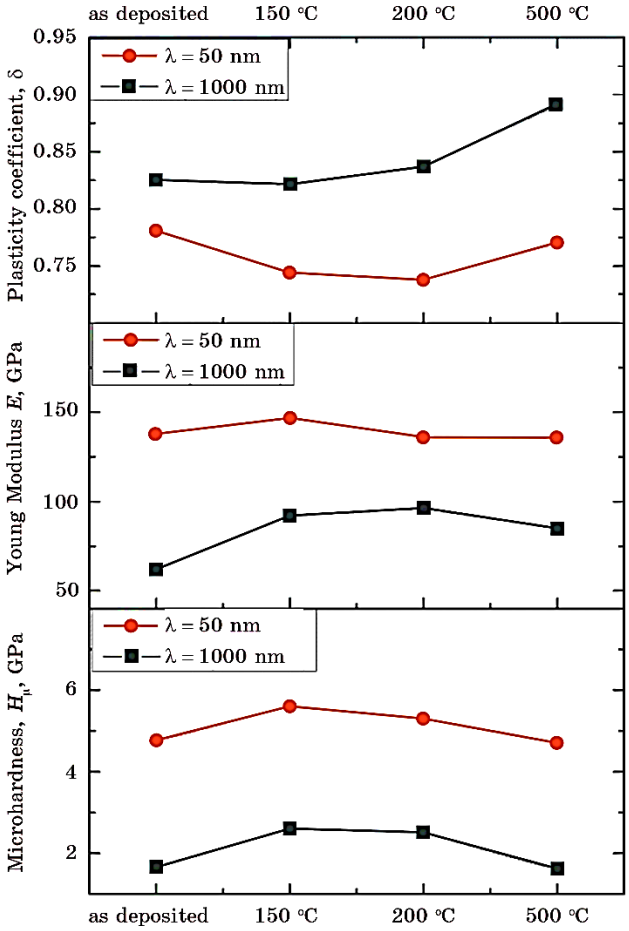

Fig. 14. Mechanical properties of foils with different modulation periods after deposition and annealing at different temperatures.

50 nm and 2.6 GPa and 92 GPa for the foil with λ of 1000 nm, respectively. The fact that the hardness of foil with a nanoscale modulation period (λ = 50 nm) after annealing at temperatures of 150°C, 200°C, and 500°C remains approximately 3 times higher than that of foil with λ = 1000 nm proves the prevailing role of the grain-boundary strengthening mechanism as compared to the interphase alloying strengthening [37].

From the viewpoint of the possible use of Al/Cu foils as filler materials for diffusion welding, it is important to study the effect of annealing on their plasticity behaviour. In particular, the plasticity coefficient of the studied foils with λ of 50 nm and 1000 nm in the initial state are 0.78 and 0.83, respectively. Annealing of the foil with λ of 50

nm at temperatures from 150°C to 200°C results in a decrease in plasticity coefficient to 0.74. In contrast, annealing of the foil with λ of 1000 nm in this temperature range only slightly decreases the plasticity coefficient to 0.82, which can be caused by the fact that the structure modification due to the formation of intermetallic Al_2Cu, Al_4Cu_9, and $AlCu_3$ phases [37, 38] in this foil is compensated by a significant contribution to the plasticity of large aluminium grains (see Fig. 6 and Fig. 7). A further increase in the annealing temperature up to 500°C led to an increase in the plasticity coefficient to 0.77 and 0.89 for foils with λ of 50 nm and of 1000 nm, respectively. The observed greater plasticity of the foil with λ =1000 nm as compared with the foil with λ = 50 nm can be due to the greater contribution from the modification of their microstructure than the phase composition which was close to the equilibrium $Al + Al_2Cu$ at the final stage of annealing.

4. CONCLUSIONS

1. It has been established that the modulation period, λ, of eutectic Al/Cu multilayer foils affects the sequence and temperature range of reactions. The observed sequence of reactions can be represented as follows:

$$Al + Cu \xrightarrow[T=100^\circ C]{} Al + Cu + Al_2Cu \xrightarrow[T=130^\circ C]{}$$
$$Al + Al_2Cu + Cu_9Al_4 \xrightarrow[T=200^\circ C]{} Al + Al_2Cu$$

for the foils with λ = 50 nm;

$$Al + Cu \xrightarrow[T=135^\circ C]{} Al + Cu + Al_2Cu + Cu_9Al_4 \xrightarrow[T=180\div215^\circ C]{} Al + Al_2Cu + Cu_3Al +$$
$$+(Cu_9Al_4) \xrightarrow[T=230^\circ C]{} Al + Al_2Cu + Cu_3Al \xrightarrow[T=390^\circ C]{} Al + Al_2Cu$$

for the foils with λ = 1000 nm.

The formation of both Al_2Cu and γ_2-Al_4Cu_9 predominantly takes place at the interphase boundaries between the Al and Cu layers, and between the Al_2Cu and Cu layers, respectively, while the formation of the β_1-$AlCu_3$ phase presumably occurs at the boundaries of columnar-like Cu grains.

2. It has been shown that, in the case of multilayer Al/Cu foils with λ = 50 nm, because of the mixing of atoms between the layers during the deposition process, supersaturated solid Al(Cu) with a copper content of about 3.1 at.% is formed. For foils with λ = 1000 nm, the formation of a solid solution with a maximum copper content of up to 2.5 at.% is observed when heated up to the reaction onset temperature. After the start of reactions for both types of foils, the copper content in the solid solution decreases to 0.5–0.6 at.%.

3. It has been established that the metastable phases β_1-$AlCu_3$ and λ_2-Al_4Cu_9 formed as a result of the reactions, as well as, in the case of the

Al/Cu foil with $\lambda = 50$ nm, the phase θ-Al_2Cu have an axial texture. In this case, the following orientational relationships are observed between the directions of textures of the initial Al and Cu phases and the formed phases:

$$<111>_{Cu} \| <111>_{Al} \| <110>_{\theta\text{-}Al_2Cu} \| <110>_{\gamma_2\text{-}Al_4Cu_9} \text{ for foils with } \lambda = 50 \text{ nm};$$

$$<111>_{Cu} \| <111>_{Al} \| <110>_{\beta_1\text{-}AlCu_3} \text{ for foils with } \lambda = 1000 \text{ nm}.$$

The presence of orientational relationships between the texture directions of the initial Al and Cu phases and the formed θ-Al_2Cu, β_1-$AlCu_3$, and γ_2-Al_4Cu_9 phases may indicate a decrease in the surface energy and energy barrier for the formation of these intermetallic compounds, which facilitates their formation.

4. It has been shown that the Al–Al_2Cu transformation leads to a decrease in the specific volume per atom by 9.8%, and the Cu–$AlCu_3$ and Cu–Cu_9Al_4 transformations lead to its increase by 3.18% and 7.29%, respectively. Analysis of the orientational relationships between the texture directions of the initial Cu phase and the formed β_1-$AlCu_3$ and γ_2-Al_4Cu_9 phases indicates a possible shear (Bain) mechanism of transformation from f.c.c. copper to structures based on the b.c.c. phase.

5. A study of the obtained Al/Cu foils using differential scanning calorimetry showed that the heat flux as a result of the exothermic reaction in foils with a short modulation period is approximately 2–2.5 times higher than in foils with a large period, which is associated with an increase in the number of reaction interfaces per unit of volume. The Kissinger method was used to determine the activation energy for the formation of the β_1-$AlCu_3$ phase in foils with $\lambda = 1000$ nm: $E_{\beta_1\text{-}AlCu_3} \cong$ $\cong 141.6$ kJ/mole $= 1.46$ eV. For the foil with $\lambda = 50$ nm, the effective activation energy was determined for a process consisting of two competing reactions with the formation of the θ-Al_2Cu and γ_2-Al_4Cu_9 phases: $E_{ef} = 124$ kJ/mole $= 1.29$ eV.

6. It has been established that the increase in the volume fraction of the intermetallic phases θ-Al_2Cu, β_1-$AlCu_3$ and γ_2-Al_4Cu_9 observed during the annealing process is accompanied by an increase in the microhardness and Young's modulus of Al/Cu multilayer foils. It has been shown that the hardness of foil with a nanoscale modulation period ($\lambda = 50$ nm) in the initial state and after annealing at temperatures of 150°C, 200°C, and 500°C remains approximately 3 times higher than that of foil with $\lambda = 1000$ nm, which indicates the prevailing role of the grain-boundary strengthening mechanism. At the same time, it was found that the plasticity of foil with $\lambda = 1000$ nm is higher than that of nanostructured foil with $\lambda = 50$ nm, which is associated with a significant contribution to the plasticity of large aluminium grains.

REFERENCES

1. B. E. Paton, A. Ya. Ishchenko, and A.I. Ustinov, *The Paton Welding Journal*, No. 12: 2 (2008).
2. A. Ustinov, L. Olikhovska, T. Melnichenko, and A. Shyshkin, *Surf. Coat. Techn.*, **202**: 3832 (2008).
3. A. I. Ustinov, Ya. I. Matvienko, S. S. Polishchuk, and A. E. Shishkin, *The Paton Welding Journal*, No. 10 (678): 29 (2009).
4. D. Turnbull, *Metal. Trans.*, **A12**: 695 (1981).
5. U. Gosele and K. N. Tu, *J. Appl. Phys.*, **53**: 3252 (1982).
6. A. E. Gershinskii, B. I. Fomin, E. I. Cherepov, and F. L. Edelman, *Thin Solid Films*, **42**: 269 (1977).
7. S. U. Campisano, E. Cosranzo, F. Scaccianoce, and R. Cristofolini, *Thin Solid Films*, **52**: 97 (1978).
8. H. G. Jiang, J. Y. Dai, H. Y. Tong, B. Z. Ding, Q. H. Song, and Z. Q. Hu, *J. Appl. Phys.*, **74**: 6165 (1993).
9. F. Haidara, M.-C. Record, B. Duployer, and D. Mangelinck, *Surface & Coatings Technology*, **206**: 3851 (2012).
10. H. T. G. Hentzell, R. D. Thompson, and K. N. Tu, *J. Appl.Phys.*, **54**: 6923 (1983).
11. H. T. G. Hentzell and K. N. Tu, *J. Appl. Phys.*, **54**: 6929 (1983).
12. J. M. Vanderberg and R. A. Hamm, *Thin Solid Films*, **97**: 313 (1982).
13. R. A. Hamm and J. M. Vandenberg, *J. Appl.Phys.*, **56**: 293 (1984).
14. J. Jellison and E. P. Klier, *Trans. AIME*, **233**: 1694 (1965).
15. T. Duguet, S. Kenzari, V. Demange, T. Belmonte, J. M. Dubois, and V. Fournee, *J. Mater. Res.*, **25**: 764 (2010).
16. C. Dong, A. Perrot, J.-M. Dubois, and E. Belin, *Mater. Sci. Forum*, **150–151**: 403 (1994).
17. C. Dong, L. M. Zhang, Q.-G. Zhou, H.-C. Zhang, J.-M. Dubois, Q.-H. Zhang, Y.-C. Fu, F.-Z. He, and F. Ge, *Bull. Mater. Sci.*, **22**: 465 (1999).
18. R. Besson, M. Avettand-Fenoel, L. Thuinet, J. Kwon, A. Addad, P. Roussel, and A. Lergis, *Acta Mater.*, **87**: 216 (2015).
19. R. Hielscher and H. Schaeben, *J. Appl. Cryst.*, **41**: 1024 (2008).
20. S. R. Ignatovich, I. M. Zakiev, D. I. Borisov, *Strength Mater.*, **38**: 428 (2006).
21. M. H. Ata, *Journal of Engineering Sciences Assut University Faculty of Engineering*, **45**: 45 (2017).
22. N. Ponweiser, C. L. Lengauer, and K. W. Richter, *Intermetallics*, **19**, Iss. 11: 1737 (2011).
23. M. Draissia and M.-Y. Debili, *Central European Journal of Physics*, **3**, No. 3: 395 (2005).
24. J. M. Zhang, and K. W. Xu, *Chinese Physics*, **13**, No. 7: 1082 (2004).
25. K.-K. Wang, *Thin Solid Films*, **717**: 138436 (2021).
26. T. Duguet, E. Gaudry, T. Deniozou, J. Ledieu, M. C. de Weerd, T. Belmonte, J. M. Dubois, and V. Fournee, *Phys. Rev. B*, **80**: 205412 (2009).
27. G. Liu, M. Gong, D. Xie, and J. Wang, *Journal of the Minerals, Metals & Materials Society*, **71**: 1200 (2019).
28. E. A. Lord and S. Ranganathan, *J. Non-Cryst. Sol.*, **334–335**: 121 (2004).
29. M. Şaşmaz, A. Bayri, and Y. Aydoğdu, *J. Supercond. Nov. Magn.*, **24**: 757 (2011).
30. G. Nolze, *Zeitschrift für Metallkunde*, **95**: 744 (2004).
31. Ya. I. Matvienko, S. S. Polishchuk, A. D. Rud, T. M. Mika, A. I. Ustinov, and

S. A. Demchenkov, *Metallofiz. Noveishie Tekhnol.*, **42**, No. 2: 143 (2020).
32. R. Besson, J. Kwon, L. Thuinet, M.-N. Avettand-Fenoel, and A. Legris, *Phys. Rev. B*, **90**: 214104 (2014).
33. V. S. Mikhalenkov, E. A. Tsapko, S. S. Polishchuk, and A. I. Ustinov, *Journal of Alloys and Compounds*, **386**, Iss. 1–2: 192 (2005).
34. L. A. Clevenger, C. V. Thompson, and R. C. Cammarata, *Appl. Phys. Let.*, **52**: 795 (1988).
35. H. E. Kissinger, *Analytical Chemistry*, **29**, Iss. 11: 1702 (1957).
36. S. Vyazovkin, *Phys. Chem. Chem. Phys.*, **28**: 18643 (2016).
37. X. Z. Wei, Q. Zhou, K. W. Xu, P. Huang, F. Wang, and T. J. Lu, *Mater. Sci. Eng. A*, **726**: 274 (2018).
38. M. Braunovic, L. Rodrigue, and D. Gagnon, *Proc. of the 54th IEEE Holm Conference on Electrical Contacts (2008)*, p. 270.